Published paper

Nano-mechanical mapping of the interactions between surface-bound RC-LH1-PufX core complexes and cytochrome c_2 attached to an AFM probe

Cvetelin Vasilev · Amanda A. Brindley ·
John D. Olsen · Rafael G. Saer · J. T. Beatty ·
C. N. Hunter

Abstract Electron transfer pathways in photosynthesis involve interactions between membrane-bound complexes such as reaction centres with an extrinsic partner. In this study, the biological specificity of electron transfer between the reaction centre-light-harvesting 1-PufX complex and its extrinsic electron donor, cytochrome c_2, formed the basis for mapping the location of surface-attached RC-LH1-PufX complexes using atomic force microscopy (AFM). This nano-mechanical mapping method used an AFM probe functionalised with cyt c_2 molecules to quantify the interaction forces involved, at the single-molecule level under native conditions. With surface-bound RC-His$_{12}$-LH1-PufX complexes in the photo-oxidised state, the mean interaction force with cyt c_2 is approximately 480 pN with an interaction frequency of around 66 %. The latter value lowered 5.5-fold when chemically reduced RC-His$_{12}$-LH1-PufX complexes are imaged in the dark to abolish electron transfer from cyt c_2 to the RC. The correspondence between topographic and adhesion images recorded over the same area of the sample shows that affinity-based AFM methods are a useful tool when topology alone is insufficient for spatially locating proteins at the surface of photosynthetic membranes.

C. Vasilev (✉) · A. A. Brindley · J. D. Olsen · C. N. Hunter
Department of Molecular Biology and Biotechnology,
University of Sheffield, Sheffield S10 2TN, UK
e-mail: c.vasilev@sheffield.ac.uk

C. N. Hunter
e-mail: c.n.hunter@sheffield.ac.uk

R. G. Saer · J. T. Beatty
Department of Microbiology and Immunology, University
of British Columbia, Vancouver, BC V6T 1Z3, Canada

Introduction

The atomic force microscope (AFM), with its picoNewton force sensitivity and nanometer spatial resolution, provides a powerful tool for exploring intermolecular forces at the single-molecule level and for mapping the topography and organisation of membrane proteins under physiological conditions (Fotiadis et al. 2002; Müller and Dufrêne 2008). AFM studies of bacterial photosynthetic membranes have revealed the membrane organisation of light-harvesting and reaction centre complexes (Scheuring et al. 2007; Sturgis et al. 2009), but this study was made possible by prior knowledge of the structures of these complexes, which made their identification relatively straightforward. However, a different approach is needed in the absence of reliable structural information and a combination of topographical and functional AFM imaging can circumvent this 'recognition' problem, most notably the PicoTREC work (combining topography and antibody-mediated protein recognition) of Hinterdorfer and co-workers (Ebner et al. 2005; Hinterdorfer and Dufrêne 2006; Chtcheglova et al. 2007) and force–volume imaging (Ludwig et al. 1997). Both methods have advantages and drawbacks; the former method lacks high time resolution, thus rendering dynamic processes effectively invisible, the latter method is reliant upon an antibody (which can be highly variable for polyclonal antibodies) to reliably recognise an antigenic motif and it also cannot quantitatively measure the interaction forces. Here, we present an imaging approach that relies upon a native protein–protein interaction found in bacterial

photosynthesis, in this case the reversible binding of an extrinsic cytochrome, (cyt) c_2, to its intrinsic membrane partner, the photosynthetic reaction centre-light-harvesting 1-PufX (RC-LH1-PufX) complex. This AFM-based imaging method is able to map the location of surface-attached RC-LH1-PufX complexes and to measure the interaction forces involved.

Cyclic photosynthetic electron transfer involves the light-induced transfer of electrons from the primary electron donor, a specialised bacteriochlorophyll dimer within the reaction centre (RC), through a series of electron acceptors to reduce a reversibly bound secondary quinone acceptor Q_B. Reduced quinone is released by the RC and oxidised by the cyt bc_1 complex, which creates a gradient of protons across the membrane. The electron transfer cycle is completed by the mobile electron carrier cyt c_2 which accepts an electron from the cyt bc_1 complex, migrates to the RC and transfers an electron to reduce the oxidised primary donor (Fig. 1). The reversible binding of cyt c_2 to the reaction centre presents an attractive model system for the study membrane-extrinsic reactions but the millisecond or sub-millisecond kinetics involved places stringent demands on the mapping methodology, requiring both high temporal resolution and the ability to quantify the interaction forces.

In this study, we apply a newly developed AFM-based technology for quantitative nano-mechanical imaging, PeakForce QNM (PF-QNM), to record single-molecule interactions between cyt c_2 molecules tethered to an AFM probe and RC-LH1-PufX core complexes immobilised onto a functionalised gold substrate. Intermolecular forces are quantified at the single-molecule level with nanometre spatial resolution. Kinetic data for the formation (Axelrod and Okamura 2005) and dissociation (Pogorelov et al. 2007) of the RC-cyt c_2 electron transfer complex were used to assess the performance of this new mapping technique. Results from PF-QNM are compared with those from conventional single-molecule force spectroscopy (SMFS), where imaging is not possible, but intermolecular forces can be measured.

Materials and methods

Protein purification

RC-His₁₂-LH1-PufX

The gene encoding a RC H protein containing 12 His residues at the carboxyl terminus was created by the SLIM procedure as described (Chiu et al. 2004). The template for mutagenesis was plasmid pTZ18U::*puhA*, (Tehrani et al. 2003) and the four oligonucleotide primers required for this mutagenesis method were: Ft, 5′-CACCACCACCACCAC CACCACCACCACCACCACCACTGATCGAGCTCTCT AGAGTCGACC-3′; Fs, 5′-CTCTAGAGTCGACCTGCA GGC-3′; Rt, 5′-AGCTCGATCAGTGGTGGTGGTGGTG GTGGTGGTGGTGGTGGTGGGCCGCCGGCGAC G-3′; Rs, GGCCGCCGGCGACGTAGCCGCA-3′. The entire mutant gene was sequenced to confirm that only the desired change was present, and the mutant gene was subcloned as a *Bam*HI to *Sac*I fragment into plasmid pATP19P, (Tehrani et al. 2003) and conjugated into the Δ*puhA* mutant strain of *Rba. sphaeroides* (Chen et al. 1998). The Δ*puhA* mutant producing the 12 His-tagged RC H protein was grown semi-aerobically in 1.5 l of M22

Fig. 1 Diagram of the electron transfer cycle in membranes of photosynthetic bacteria. The mobile electron carrier cyt c_2 accepts an electron from the cyt bc_1 complex and migrates to the RC and transfers an electron to reduce the oxidised primary donor

liquid culture containing 1 mg ml^{-1} of tetracycline at 34 °C for 2 days in a shaker incubator (in the dark at 180 rpm). The 1.5 l culture was harvested by centrifugation (5,300 g/25 min in a Beckman JA-10 rotor at 4 °C), and the cell pellet was re-suspended in 15 ml of 10 mM HEPES pH 7.4 buffer. The concentrated cell suspension was frozen at −20 °C until immediately prior to French press disruption. The cells were pre-treated with lysozyme (0.7 mg ml^{-1} final concentration) and incubated at 37 °C for 30 min. DNase I was added to the cells prior to lysis and the pressing was conducted at a cell pressure of 2.9 MPa in an Aminco French pressure cell. The pressing was repeated for maximum lysis. The lysate was loaded onto a 15 %/40 % (wt/wt) sucrose step gradient and centrifuged in a Beckman Ti 45 rotor for 10 h at 57,000×g at 4 °C. The intracytoplasmic membrane fraction was harvested from the interface and further treated to concentrate the membranes by diluting out the sucrose with 10 mM HEPES pH 7.4 buffer and centrifuging in a Beckman Ti 45 rotor for 2 h at 125,000×g at 4 °C. The membrane pellet was re-suspended in a small volume, typically 1 ml of 10 mM HEPES pH 7.4 buffer, and frozen at −20 °C for further use. The membrane pellet obtained from sucrose gradient centrifugation were solubilised with *n*-dodecyl-*beta*-D-maltoside (β-DDM, Glycon) at a final concentration of 59 mM, and a final OD of the membrane sample of ∼60 at 875 nm. The mixture was stirred at 4 °C in the dark for 90 min. Non-solubilised material was removed by centrifugation (in a Beckman Ti 45 rotor for 2 h at 125,000×g), and the supernatant was loaded onto Chelating Sepharose Fast Flow Ni–NTA column (GE Healthcare) equilibrated with 10 mM HEPES pH 7.4, 500 mM NaCl, 10 mM Imidazole, 0.59 mM β-DDM buffer. A gradient of 10–400 mM imidazole was applied and the main peak, which contains pure His$_{12}$-RC-LH1-PufX, appeared when the concentration of imidazole reached ∼300 mM. Eluted protein was concentrated (Vivaspin 500 spin-concentrator, Sartorius) and dialyzed against 10 mM HEPES pH 7.4, 50 mM NaCl, 0.59 mM β-DDM buffer. Then, the RC-His$_{12}$-LH1-PufX protein was loaded onto a DEAE-Sepharose (Sigma) ion-exchange column equilibrated with 10 mM HEPES pH 7.4, 50 mM NaCl, 0.59 mM β-DDM buffer. A gradient of 50–300 mM NaCl was applied with the main peak of pure protein appearing at NaCl concentration of ∼280 mM. The best fractions judged from the peak absorbance ratio of 875–280 nm were pooled (A_{880}/A_{280} ∼ 1.9). The protein was again concentrated and dialyzed against 10 mM HEPES pH 7.4, 50 mM NaCl, 0.59 mM β-DDM buffer and applied to a HPLC column (Phenomenex BioSep) and eluted at a flow rate of 0.3 ml min^{-1} in order to separate the monomeric and dimeric RC-His$_{12}$-LH1-PufX complexes. The second elution peak (corresponding to the monomeric fraction of

RC-His$_{12}$-LH1-PufX) was collected, concentrated to a final concentration of 15 μM in 10 mM HEPES pH 7.4, 50 mM NaCl, 0.59 mM β-DDM buffer and stored at −80 °C for further use.

Cyt c$_2$-His$_6$

The gene encoding cyt c$_2$ was amplified from genomic DNA from *Rba. sphaeroides* 2.4.1 strain using a 5′ primer TCGAATTCATGTCATGCATGATCCGGAACG which contains an *Eco*RI site for cloning into the pRK415 plasmid and a 3′ primer AAGCTTTCAGTGGTGGTGGTGGT GGGGGGCCGGACGGCGACCTGCTGG which includes a His$_6$ sequence for immobilised metal ion affinity chromatography (*IMAC*) and a *Hin*dIII site for cloning into pRK415 plasmid. The gene was cloned using Touchdown PCR and sub-cloned into the pRK415 vector using *Eco*RI and *Hin*dIII restriction sites for directional cloning. The plasmid with the gene was then mated into a ΔcycA strain of *Rhodobacter sphaeroides* via *Escherichia coli* S17 (Simon et al. 1983). The intracytoplasmic membrane fraction from the cyt c$_2$-His$_6$ mutant was prepared in exactly the same way as described in the paragraph above. The membrane pellet obtained from sucrose gradient centrifugation was solubilised with *N,N*-dimethyldodecan-1-amine oxide (LDAO, Fluka) at a final concentration of 65 mM, and a final OD of the membrane sample of ∼80 at 875 nm. The mixture was stirred at room temperature in the dark for 20 min. Non-solubilised material was removed by centrifugation (in a Beckman Ti 45 rotor for 2 h at 125,000×g), and the supernatant was loaded onto Chelating Sepharose Fast Flow Ni–NTA column (GE Healthcare) equilibrated with 10 mM HEPES pH 7.4, 500 mM NaCl, 10 mM Imidazole, 1 mM LDAO buffer. A gradient of 10–400 mM imidazole was applied and the purified cyt c$_2$-His$_6$ eluted when the concentration of imidazole reached ∼270 mM. The purified protein (A_{414}/A_{280} ratio ≥3.3) was dialyzed against 10 mM HEPES pH 7.4, 50 mM NaCl, 1 mM LDAO buffer, concentrated to a final concentration of 740 μM and stored at −80 °C for further use.

AFM probes and sample substrates functionalization

Epitaxially grown Au [111] thin layers (PHASIS, Switzerland) were functionalised, as received and without further treatment, with mixed EG$_3$/Ni–NTA thiol self-assembled monolayer. Hybrid AFM probes, Si tips mounted on Si$_3$N$_4$ triangular cantilevers, model SNL or MSNL (Bruker), were first cleaned by washing in acetone (HPLC grade, Fisher Scientific) and then cleaned in a home-built UV/Ozone cleaner (LSP035 Pen-Raylight source, LOT-Oriel Ltd.) for 45 min. Immediately after the cleaning step the AFM probes were placed into a thermal evaporator (Auto 306,

Edwards, UK) and were coated first with $\sim$4 nm of adhesive chromium layer, followed by $\sim$30 nm of gold layer on the tip side. After that the AFM probes were functionalised with mixed EG_3/Ni–NTA thiol SAM. Briefly, both the gold substrates and the AFM probes were immersed in an ethanolic solution of EG_3-thiol ((11-Mercaptoundecyl)tri(ethylene glycol), Sigma-Aldrich) and Ni–NTA-thiol (HS-C11EG3-NTA from ProChimia Surfaces Sp. z o.o., Poland) mixed at a ratio of either 1:200 (mol/mol)—when used for substrate functionalization—or 1:5 (mol/mol) when used to functionalised AFM probes with a final total concentration of thiols of 1 mM. The functionalization was carried out for 16 h with subsequent wash in pure HPLC grade ethanol (Sigma-Aldrich). In the next step, the NTA end-groups of the monolayer were charged with Ni^{2+} ions by incubation in 70 mM aqueous solution of $NiSO_4$ with subsequent washing of the substrates and the AFM probes in pure water. In the final step, the RC-His_{12}-LH1-PufX and cyt c_2-His_6 proteins were attached to the gold substrates and the AFM probes, respectively. This was achieved by incubating the functionalised gold surfaces in a solution of RC-His_{12}-LH1-PufX in 10 mM HEPES pH 7.4, 250 mM KCl, 0.59 mM β-DDM for 15 min and then very gently washing the samples (4 times) in 10 mM HEPES pH 7.4, 250 mM KCl, 0.59 mM β-DDM buffer and storing them in imaging buffer for further use. Different concentration of RC-His_{12}-LH1-PufX was used to control the surface density of the molecules. A final concentration of 65 nM was used to achieve surface density of 200–300 molecules per μm^2 and a final concentration of 800 nM resulted in much denser coverage of the sample surface used in SMFS experiments. The AFM probes were incubated with a 30 μM solution of cyt c_2-His_6 for 15 min and then extensively washed in 10 mM HEPES pH 7.4, 250 mM NaCl, 1 mM LDAO buffer to remove the physisorbed protein. Next, the AFM probes were washed and stored in imaging buffer. In parallel with the AFM probes, gold substrates were functionalised in exactly the same way (at the same time with the AFM probes). This helped us to assess the final surface density of the protein molecules attached to the AFM probes. We estimated that there are about 100–150 molecules attached to the active area on the apex of the AFM probe (defined as the part of the apex of the tip where the attached protein molecules can be brought into contact with the proteins on the surface). The surface area of that part of the tip is nominally around 22,000 nm^2 in this case.

AFM measurements

All AFM measurements were performed with a Multimode 8 instrument equipped with a NanoScope V (Bruker) controller. NanoScope (v 8.15) software (Bruker) was used for data collection. PeakForce QNM measurements were performed in imaging buffer (10 mM HEPES pH 7.4, 45 mM KCl) at room temperature using SNL (cantilever C) probes (Bruker). The spring constant for each cantilever was obtained using the built-in cantilever calibration (thermal method) in the NanoScope software; the obtained spring constants for the cantilevers used were in the range 0.121–0.18 N m^{-1}. The Z-modulation amplitude was adjusted to values in the range 20–25 nm to allow enough tip–sample separation in order to fully separate the cyt c_2-His_6 from the RC-His_{12}-LH1-PufX molecules on the surface during each ramp cycle. The Z-modulation frequency (repetition rate) was 1 kHz and the contact tip–sample force was kept in the range 100–150 pN. The imaging rate was adjusted in a way that ensured two force–distance curves recorded per image pixel. The pixel size is about 2 nm for the PF-QNM data so given the size of the RC it can be contacted up to 4–6 times by the cyt c_2 molecules as the AFM probe is scanned over the sample (bearing in mind that the 'binding efficiency' of the tethered molecules in our experiment is lower compared to free molecules in solution). Conventional force–distance measurements were performed under the same conditions as described before using MSNL (cantilever E) probes (Bruker) with spring constants in the range 0.082–0.114 N m^{-1}. The ramp size was 250 nm with a constant approach velocity of 500 nm s^{-1}, the dwell time (i.e. the interval between approach and retraction) set equal to zero and the retract velocity was 500 nm s^{-1} and a repetition rate of 1 Hz. The contact force was kept at a low value, below 150 pN.

During all AFM measurements (with the exception of the dark control measurements) the sample and the AFM probe were illuminated from a white light source through an optical fibre (Fiber-Lite MI-150, Dolan-Jener) and the power density of the illumination at the sample surface, approximately 11 W m^{-2}, was measured with a Newport 842-PE (Newport Corp.) power meter. This illumination allowed for the repeated photo-oxidation of the RC-His_{12}-LH1-PufX protein immobilised on the sample surface after each electron transfer interaction with the cyt c_2-His_6 proteins on the AFM probe. Before starting the measurements, the cyt c_2-His_6 proteins on the AFM probe were pre-reduced by incubation in reducing buffer (imaging buffer supplemented with 0.5 mM sodium dithionite and 0.25 mM phenazine methosulfate, both chemicals from Sigma-Aldrich) with a subsequent wash in imaging buffer. In order to ensure stable specific interactions between the proteins attached to the sample surface and their redox partner on the AFM probe after acquiring two to three AFM scans or a series of force–distance curves, the AFM probe was consecutively washed in reducing and imaging buffer, and used again.

For the control experiments, the RC-His_{12}-LH1-PufX protein was chemically reduced (treated with imaging buffer supplemented with 0.5 mM sodium dithionite and 0.25 mM phenazine methosulfate), then washed in imaging

buffer and imaged in the dark. In this case, the control AFM measurements were conducted in a dark box with the only illumination to the sample and the AFM probe being the 639 nm laser used in the optical lever detection system for the AFM. Alternatively, the docking site of the RC-His$_{12}$-LH1-PufX protein on the sample surface was blocked by injection of a tenfold molar excess of free pre-reduced cyt c_2-His$_6$ directly into the AFM imaging cell.

Data analysis

All the AFM data was analysed using Gwyddion v 1.29 (open source software covered by GNU general public license, www.gwyddion.net), Nanoscope Analysis v 1.42 (Bruker), PUNIAS v1r15 (www.punias.voila.net) and OriginPro v8.5.1 (OriginLab Corp.) software. Gwyddion and Nanoscope Analysis were used for image processing and analysis. Nanoscope Analysis was also used for the extraction of the force data from the nano-mechanical adhesion images. PUNIAS and OriginPro 8.5 were used for the statistical analysis of all the force spectroscopy data and OriginPro was also used for all the calculations and fittings.

Data reduction (positive identification of specific rupture events) was based on the identification of rupture events occurring at tip–sample separation in the range 2–6 nm; all force–distance curves exhibiting rupture events outside that range were discarded. The most probable values for the unbinding forces were obtained from the maximum of the Gaussian fit to the force distribution combined in a statistical histogram. Normally, the rupture forces of a few hundred rupture events were compiled in force or loading rate distribution histograms.

Results

Surface-immobilised RC-LH1-PufX protein complexes

An epitaxial gold surface was functionalised with a self-assembled monolayer of a mixture of alkanethiols with polyethylene glycol (EG$_3$) and nitrilotriacetic acid (NTA) functional end-groups. The monomeric RC-LH1-PufX core complex was attached to the NTA-alkanethiols via a C-terminal His$_{12}$-tag on the RC H-subunit. Cyt c_2 molecules, each also carrying a C-terminal His$_6$-tag, were immobilised onto a gold-coated (on the tip side) AFM probe also functionalised with a mixed EG$_3$/NTA thiol monolayer (Fig. 2). The His-Ni^{2+}-NTA coordination bond has been demonstrated to provide the appropriate orientation and high mobility when coupling biological molecules (Dupres et al. 2005; Verbelen et al. 2007). In addition, the presence of EG$_3$ end-groups in the mixed monolayer minimises the non-specific adsorption/interactions between the protein
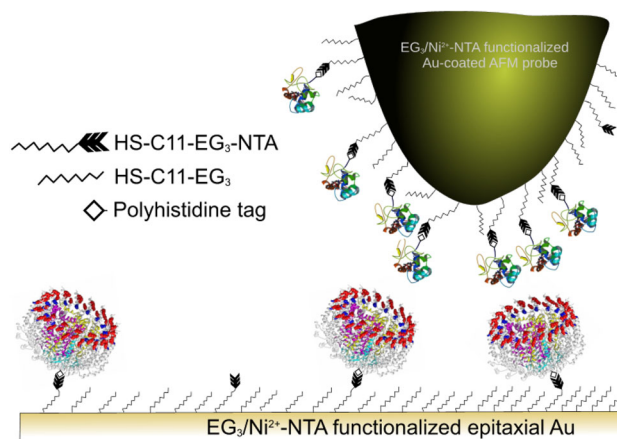
Fig. 2 Protein complex attachment chemistry. Schematic representation of the immobilised proteins on the AFM probe and sample substrate: The RC-His$_{12}$-LH1-PufX core complexes are immobilised via His$_{12}$-Ni^{2+}-NTA coordination bond on functionalised epitaxial gold substrate. The surface density of the molecules is ~250–350 molecules per µm^2. The cyt c_2-His$_6$ molecules are attached to a functionalised gold-coated AFM probe again via His$_6$-Ni^{2+}-NTA coordination bond at much higher surface density of around 5,000–6,000 molecules per µm^2

complexes and the surface or AFM probe (Vanderah et al. 2004).

The surface density of the immobilised RC-His$_{12}$-LH1-PufX molecules on the functionalised epitaxial gold surface was found to be in the range 250–350 molecules per µm^2, while the surface density of the cyt c_2-His$_6$ molecules attached to the functionalised AFM probe was estimated to be much higher, in the range of 5,000–6,000 molecules per µm^2. This is equivalent to 100–150 cyt c_2-His$_6$ molecules for the active area of the tip (see "Materials and methods").

Functional AFM imaging of the interactions between monomeric RC-His$_{12}$-LH1-PufX core complex and the cytochrome c_2 electron carrier

In order to visualise the interactions between the protein molecules on the sample surface and their redox partners on the AFM probe, we used a non-resonant oscillatory AFM imaging mode, PF-QNM, where the probe taps the sample surface and generates force–distance curves at each pixel of the image, thus providing, together with high-resolution topography images, quantitative mechanical characterisation (elasticity, deformation, adhesion, dissipation) of the sample with nanometer resolution (Patent No. US 2010/0122385 A1). Of particular interest is the adhesion data which measures the forces arising from the forced dissociation of the RC-His$_{12}$-LH1-PufX-cyt c_2-His$_6$ complex upon the separation (retraction) of the AFM probe from the surface. Both the topography and the adhesion data were recorded simultaneously, thus imaging the surface distribution of the molecules while monitoring the interactions between the two proteins.

A topography image (Fig. 3a) was recorded at modulation frequency of 1 kHz, in imaging buffer (45 mM KCl, 10 mM HEPES pH 7.4) and under white light illumination with a power density of approximately 11 W m^{-2} (measured at the sample surface) in order to ensure the photo-oxidation of the RC-His$_{12}$-LH1-PufX special pair and to favour binding of the reduced cyt c_2-His$_6$ electron donor attached to the functionalised AFM probe. Individual RC-His$_{12}$-LH1-PufX complexes can be clearly seen on the gold substrate with an average height of around 7 nm and a lateral size (FWHM) in the range 16–20 nm (inset in Fig. 3a), consistent with the expected size ($\sim$12 nm) of the monomeric RC-His$_{12}$-LH1-PufX complex and taking into account increased lateral dimensions due to geometrical tip convolution effects. Notably, some larger aggregates (of 2 or 3 core complexes) are also visible on the surface, indicated by the red arrows in Fig. 3a. Simultaneously with the topography, an adhesion image was recorded (Fig. 3c), where we can easily identify the high adhesion (or high unbinding force) events, highlighted in red, resulting from forced dissociation of the cyt c_2-RC-His$_{12}$-LH1-PufX complexes while they are still in a transient bound state. The total number of molecules on the surface in Fig. 3a is 209 and the total number of high unbinding force events in the corresponding adhesion image is 137, giving a binding frequency, under these experimental conditions, of approximately 66 %. In order to estimate the magnitude of the interaction forces between the two molecules, we measured the forces corresponding to each of the unbinding events in Fig. 3c, and the histogram of the interaction force distribution (inset in Fig. 3c) gave a mean value of 483.3 $\pm$ 9.8 pN (mean $\pm$ SE). The good correlation between the unbinding events and the position of the RC-His$_{12}$-LH1-PufX molecules on the surface is highlighted in Fig. 3e by combining the topography and adhesion images in a 3D composite image, where the profile represents the sample topography and the colour coding indicates the strength of the interaction forces. The slight offset of the high unbinding force events from the centres of the RC-His$_{12}$-LH1-PufX molecules is most likely result from interaction with cyt c_2-His$_6$ molecules attached with an offset (not directly at the apex) to the AFM tip, together with a scan direction artefact during the image acquisition.

Since interaction with the tip-bound reduced cyt c_2-His$_6$ requires that the surface-bound RC-His$_{12}$-LH1-PufX complexes are in the oxidised state, (RC[ox]), we performed a control experiment by chemically reducing the RC-His$_{12}$-LH1-PufX complex while conducting the AFM measurements in the dark to prevent RC photo-oxidation. Topographic and adhesion images were recorded over exactly the same area of the sample: the topography of the sample, Fig. 3b, is unchanged while the 137 high unbinding force events in the adhesion map, Fig. 3d, decreases to only 25—a significant drop by a factor of 5.5. This is an unambiguous indication that the high adhesion force events we observed in the adhesion images are associated with a specific interaction promoted by photooxidation of the RC. It is worth noting that some high-force unbinding events remained unaffected by the change in the redox conditions, indicated with the black arrows in Fig. 3c, d, but they do not correlate with RC-His$_{12}$-LH1-PufX molecules as evident from the 3D composite representations in Fig. 3f.

Single-molecule force spectroscopy study of the interactions between monomeric RC-LH1-PufX core complex and the cytochrome c_2 electron carrier

PF-QNM is a new method for simultaneously imaging the surface topography and the distribution of intermolecular forces, but there is a more established method, SMFS, for quantifying intermolecular forces (Bonanni et al. 2005), although not their surface distribution. Although the mapping aspect is an important part of our aims the conventional SMFS approach still provides a useful validation of our experimental system, and of the specificity of the interactions observed between the RC-His$_{12}$-LH1-PufX and cyt c_2 proteins. In the conventional force spectroscopy experiment, the molecule (or molecules) attached to the AFM probe is brought briefly into contact with the partner molecules on the surface and after a short dwell time the molecules are separated while continuously recording the forces acting on the AFM probe. Typical force–distance curves recorded during such experiment are represented in Fig. 4a. These data were recorded on a sample similar to that used for the nano-mechanical mapping, namely RC-His$_{12}$-LH1-PufX molecules immobilised on EG$_3$/Ni^{2+}-NTA-functionalised gold surfaces, but at a much higher surface density of $\sim$4,000 molecules per μm^2 (see Fig. 4b). For comparison, a tightly packed monolayer of RC-His$_{12}$-LH1-PufX complexes 12 nm in diameter would represent nearly 7,000 molecules per μm^2. The particular set of force–distance curves in Fig. 4a clearly displays unbinding events with rupture lengths in the range 2–5 nm and rupture forces in the range 165–225 pN. Typically, series of around 1,000 force–distance curves were recorded over different locations of the sample under conditions that favour or disfavour the binding of the probe-bound cyt c_2 to RC-His$_{12}$-LH1-PufX complexes. Each series of force–distance curves was analyzed to evaluate the distribution of the separation forces acting between the two proteins as well as the binding frequency under different conditions (see "Materials and methods").

In order to exclude the non-specific interactions from our force spectroscopy experimental data, we also performed a control measurement with a functionalised AFM probe (cyt c_2-His$_6$ attached to the tip) on a bare EG$_3$/Ni^{2+}-NTA-functionalised gold surface with no immobilised RC-His$_{12}$-LH1-PufX complexes (Fig. 4d). In order to clearly
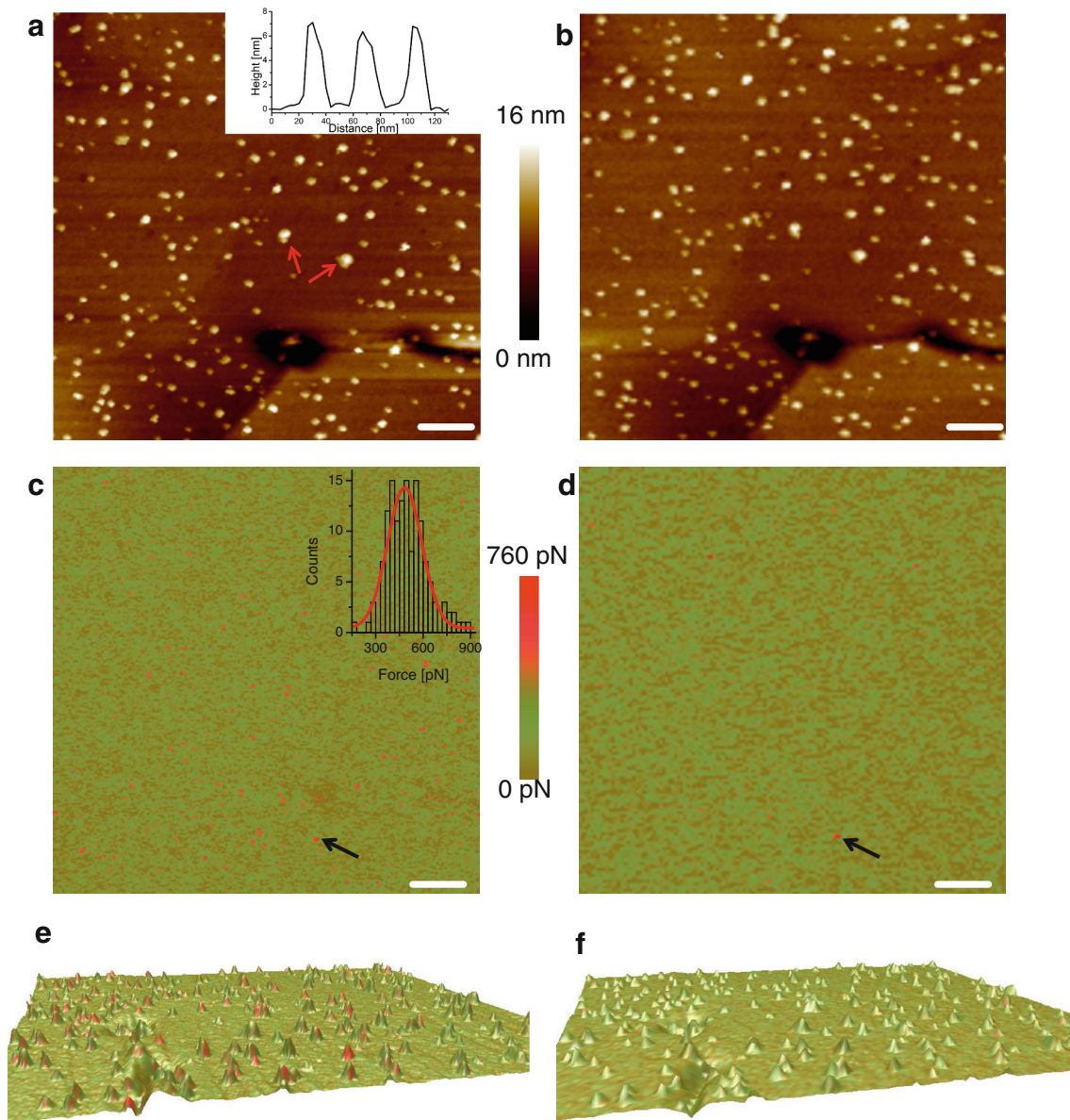
Fig. 3 Functional AFM imaging of the interaction between RC-LH1-PufX and cyt c_2. **a** and **c** AFM topography image of individual RC-His$_{12}$-LH1-PufX core complexes immobilised on a functionalised gold surface (*inset* in **a** shows the height and lateral size of the core complex molecules along the *dashed line*) and the corresponding adhesion image. The histogram (*inset*) in **c** shows the distribution (with the Gaussian fit in *red*) of the specific interaction forces recorded in the adhesion image; the mean value is approximately 483 pN; **b** and **d** AFM topography image and the corresponding adhesion image of the same area of the sample after chemically reducing the core complexes on the surface and imaging in the *dark*. The *black arrows* in **c** and **d** indicate two high-force non-specific interactions that were not affected by the change in the redox conditions; **e** 3D composite images (topography combined with adhesion skin) of the specific unbinding events from **a** and **c**; **f** as for **e**, but with data from **b** and **d**. In panels **c**–**f**, the colour coding is as follows: the *red colour* corresponds to the specific events (high unbinding force), while the *beige colour* corresponds to the non-specific interactions. The *scale bar* in all *panels* is 100 nm

show the difference between the rupture events occurring when separating the RC-His$_{12}$-LH1-PufX and cyt c_2 proteins and the non-specific interactions in our experiment, a typical set of force–distance curves recorded over the clean EG$_3$/Ni^{2+}-NTA-functionalised gold substrate is shown in Fig. 4c, exhibiting lower rupture forces.

The histogram in Fig. 5a shows the distribution of the rupture forces measured from 261 unbinding events over 880 force–distance curves recorded under photo-oxidative conditions (white light illumination). This gives a binding frequency of approximately 29 %. The best Gaussian fit of the histogram gives two values for the most probable

a

b

c

d
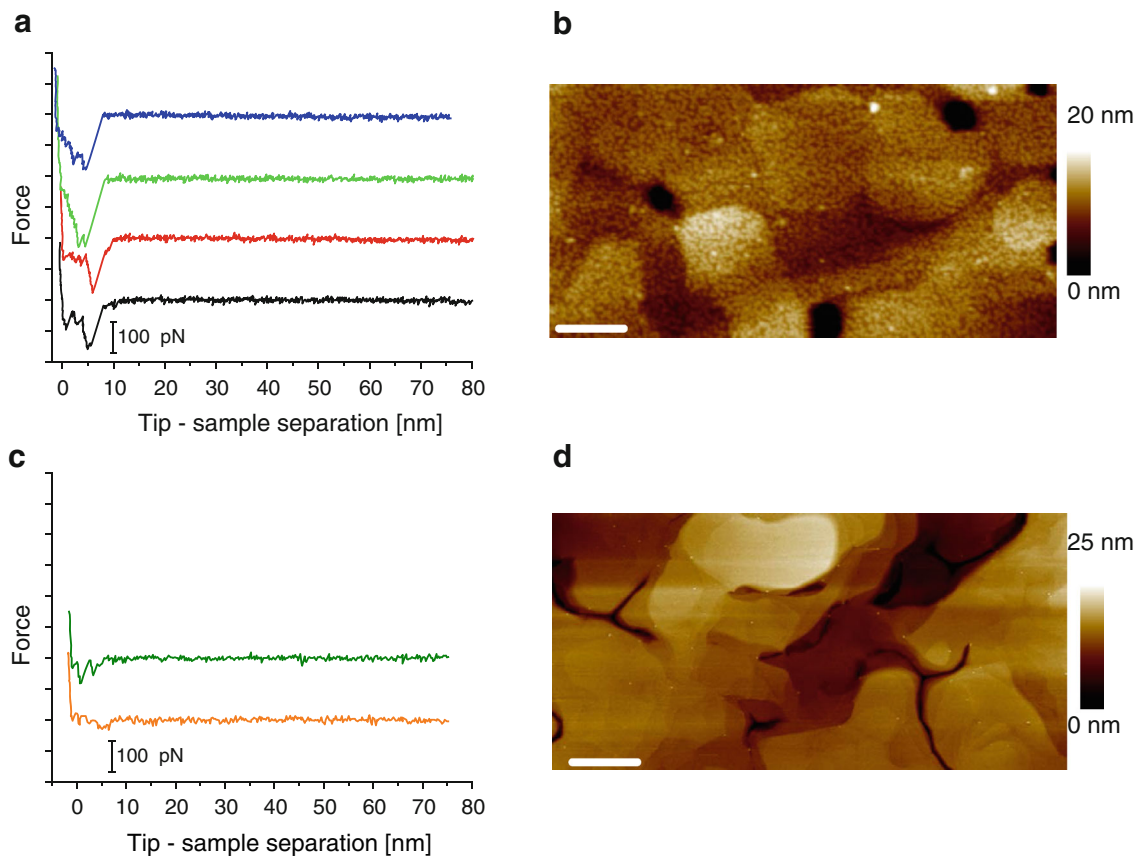
Fig. 4 Conventional force spectroscopy. **a** Typical force–distance curves recorded upon the retraction of the AFM probe functionalised with pre-reduced cyt c_2-His$_6$ under white light illumination recorded on a gold surface densely covered with immobilised RC-His$_{12}$-LH1-PufX; **b** AFM topography image of a functionalised gold surface densely covered with immobilised RC-His$_{12}$-LH1-PufX; **c** typical force–distance curves recorded with cyt c_2-His$_6$-functionalised AFM probe under the same conditions as the data in **a** but on a clean EG$_3$/Ni^{2+}-NTA-functionalised gold surface (no RC-His$_{12}$-LH1-PufX immobilised on it); **d** AFM topography image of a clean EG$_3$/Ni^{2+}-NTA-functionalised gold surface. The *scale bar* for the topography images in **b** and **d** is 500 nm. For clarity the force–distance curves in **a** and **c** are offset along the Y-axis; the *scale bar* for the Y-axis is 100 pN

unbinding force, 164 ± 19 and 305 ± 25 pN (mean $\pm$ SE), respectively.

In order to test the inhibition of the formation of a transient bound state between the RC-His$_{12}$-LH1-PufX and cyt c_2-His$_6$ proteins, we performed a control experiment similar to that used for the PF-QNM by recording a series of force–distance curves on a RC-His$_{12}$-LH1-PufX complex (immobilised on functionalised gold substrate) chemically reduced in the dark to prevent RC photo-oxidation. Analysis of the force data recorded under these conditions revealed a dramatic drop in the binding frequency—only 101 force–distance curves out of 1,495 exhibited rupture events resulting in a binding frequency of 6.7 % with no prominent peak observable in the force distribution histogram, Fig. 5b.

The docking site on the photooxidised RC-His$_{12}$-LH1-PufX was blocked with pre-reduced cyt c_2-His$_6$ molecules that were injected into the AFM liquid cell at a final concentration of 3 μM, an order of magnitude higher than the

K_D of ~ 0.3 μM (Tetreault et al. 2001). Analysis of the data obtained after the blocking with free cyt c_2-His$_6$ revealed a weak peak at around 180 pN in the force distribution histogram with a binding frequency of 8.8 % (140 rupture events out of 1,590 force–distance curves), Fig. 5c. This residual binding probability in the blocking control is likely to arise from repeated binding and unbinding events between the RC-His$_{12}$-LH1-PufX complex on the sample surface and the free cyt c_2-His$_6$ in solution that leave the RC binding site unblocked for short periods. Thus, each cyt c_2 docking site on the surface-bound RCs is transiently available to interact with cyt c_2 on the probe, although with a much reduced probability (29 % down to 8.8 %). Finally, the distribution of the forces recorded using a clean EG$_3$/Ni^{2+}-NTA-functionalised gold substrate, with no RC-His$_{12}$-LH1-PufX complexes (Fig. 5d) gives no prominent peak in the histogram and the data reveal a very low frequency (~ 6 %) for interaction, with only 60 rupture events out of 950 force–distance curves.
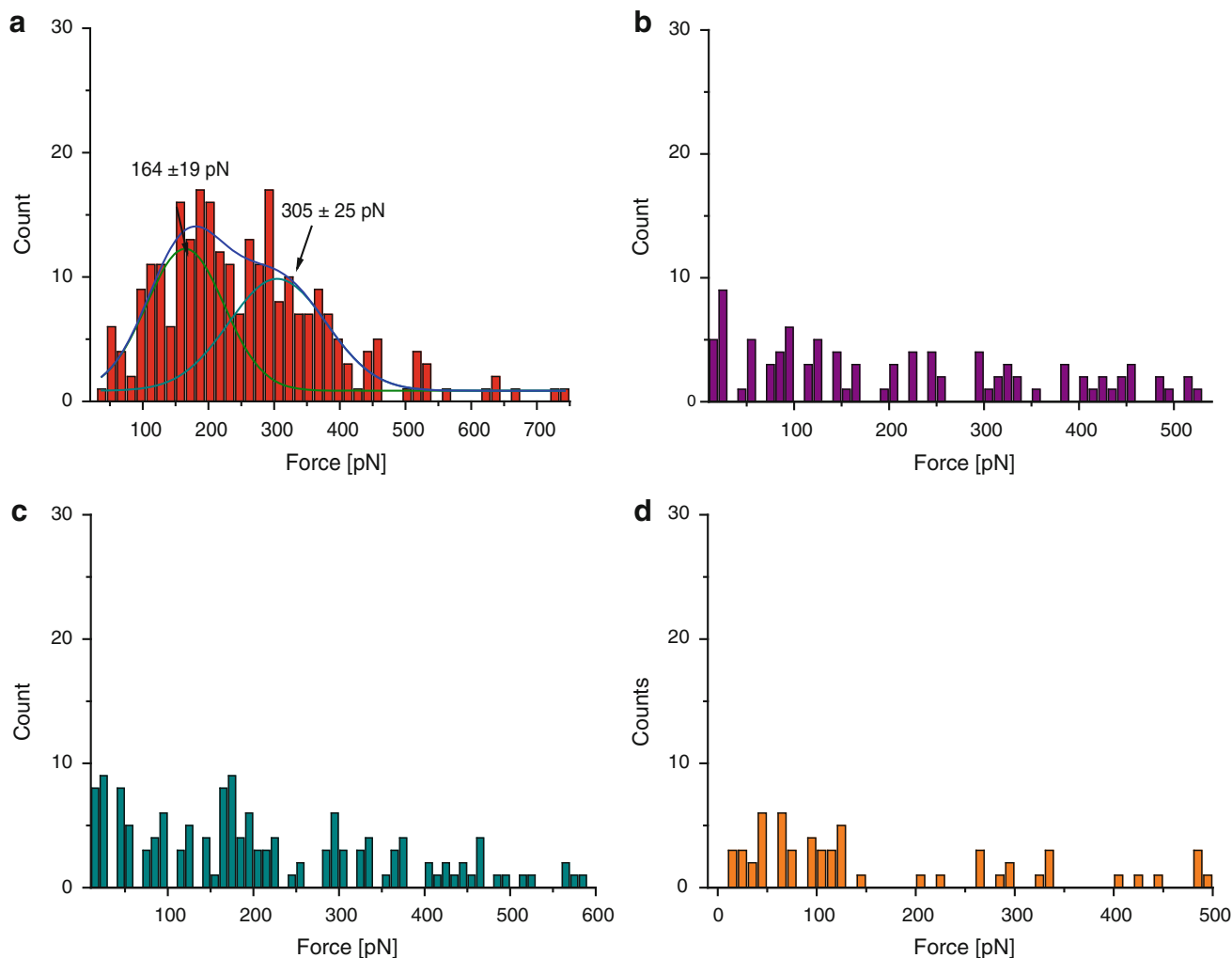
Fig. 5 Specificity of the unbinding events. **a** Force distribution (most probable force obtained from the Gaussian fit, *blue curve*) for the specific unbinding between RC-His$_{12}$-LH1-PufX and the cyt c_2-His$_6$ under white light illumination; **b** control measurements: distribution of forces measured on chemically reduced RC-His$_{12}$-LH1-PufX complex (RC[*red*]) in the *dark*; **c** control measurements: blocking the docking site RC-His$_{12}$-LH1-PufX with free c_2-His$_6$ injected during the force measurements; **d** control measurements: histogram showing the distribution of interaction forces measured between the cyt c_2-His$_6$-functionalised AFM probe and a clean EG$_3$/Ni^{2+}-NTA-functionalised gold substrate

Discussion

The cyt c_2 docking site on the RC is surrounded by the extrinsic C-terminal regions of the LH1 complex. For each half of the dimeric RC-LH1-PufX complex there are 14 LH1 αβ polypeptide pairs, with each C-terminal domain bearing 4 negative and 3 positive charges, including the C-terminal carboxylates. We suggest that the presence of a circular array of 98 charges, with a net charge of −14, could restrict the possible pathways for association and dissociation between the cyt c_2 and the periplasmic surface of the RC. It seems likely that, when leaving the docking site on the RC, the cyt c_2 has to migrate out of plane (perpendicular to the membrane surface) in order to be able to evade the LH1-charged residues. This probable pathway coincides with the pulling trajectory in our experiments (both PF-QNM and SMFS).

The His-Ni^{2+}-NTA coordination chemistry used in these experiments can achieve long-lasting attachment of proteins (several thousand force–distance cycles, up to several hours) to a functionalised AFM probe or surface, while sustaining significant force stresses (up to 500 pN) (Schmidt et al. 2002; Conti et al. 2000; Nevo et al. 2003; Berquand et al. 2005; Dupres et al. 2005) without the need of a covalent chemical linkage, thus preserving the protein structure and functionality. The unbinding forces measured during the PF-QNM experiments, approximately 480 pN, are close to the estimated values in a theoretical study of the pathways for cyt c_2–RC-LH1-PufX interaction, with forces in the range 600–1,000 pN (Pogorelov et al. 2007). It

is worth noting the fact that purified RC-LH1-PufX complexes were found to retain 25–30 % of the endogenous quinone acceptor pool (Comayras et al. 2005). This quinone pool stores the electrons resulting from the photo-oxidation of the primary donor, thus maintaining the turnover of the electron transfer cycle during image acquisition.

Cyt c_2 to RC electron transfer is in the low microsecond range (Overfield et al. 1979; Moser and Dutton 1988) so, having being brought into contact with a surface-bound RC, the cyt c_2 will be immediately oxidised, given the dwell time of $\sim$160 μs (PF-QNM) or several milliseconds (SMFS). Thus, the interaction sampled by the unbinding events is likely to be between RC[red] and an oxidised cyt c_2 (cyt c_2[ox]). The negative control shows that a cyt c_2[red]–RC[red] interaction has a low probability. The more probable interaction arises when the initial states (prior to the tip-surface encounter) consist of reduced cyt c_2 and oxidised reaction centres. Therefore, it appears that the cyt c_2-RC association is maintained in the aftermath of the initial electron transfer event, although the oxidised cyt c_2—reduced RC control, which would have helped dissect the nature of the complex, was not performed. This study does, however, probe the long-lived forces that stabilise the cyt c_2–RC association, under controlled conditions of force and distance.

Chemical reduction of the RC-His$_{12}$-LH1-PufX complex in the dark prevents formation of the photo-oxidised electron acceptor state, resulting in a more than fivefold reduction in the frequency of cyt c_2-RC rupture events. This large difference indicates that the unbinding events we have observed and analysed with photo-oxidised RCs involve the formation of the electron transfer complex between the cyt c_2 and RC-LH1-PufX proteins at some stage during our measurements. The results from our SMFS control experiments with a large excess of free cyt c_2-His$_6$ in solution are consistent with this conclusion; here, the binding probability decreased by the same factor down to the level of the probability for a non-specific interaction. In the latter case, the residual binding probability in these control measurements can be attributed to the dynamic nature of the interaction between the RC-His$_{12}$-LH1-PufX complex on the sample surface and the free cyt c_2-His$_6$ in solution, which, although in excess, still leaves the RC binding site unblocked for short periods and free to interact with surface-bound cyt c_2-His$_6$ molecules.

In the two types of AFM experiments performed here, PF-QNM and SMFS measurements, experimental parameters such as the tip–sample contact time (defined as the time interval between bringing both molecules together and their complete separation), the approach and retract velocities of the AFM probe and the repetition rate of the measurement differ substantially, thus not always allowing

for direct comparison between the data. During the PF-QNM measurement, the tip–sample contact time is approximately 160 μs and the repetition rate of the force measurements is 1 kHz. The tip–sample contact time is shorter than the half-life time of the bound state of the electron transfer complex, which is approximately 200–400 μs (Dutton and Prince 1978; Overfield et al. 1979). Moreover, the repetition rate of the force measurements is 1 kHz, higher than the maximum possible turnover rate, which is in the range 270–800 s^{-1} (Gerencsér et al. 1999; Paddock et al. 1988). Thus, we can conclude that the PF-QNM measurements do not undersample the dissociation events but rather oversample them, indicating that PF-QNM experiments can access the transient bound state of the electron transfer complex and measure the dissociation of its components. Nevertheless, we cannot distinguish between cyt c_2[ox]–RC[red] and cyt c_2[red]–RC[ox] interacting pairs, given that the duration of tip–sample contact of approximately 160 μs is much longer than the time taken for electron transfer (Overfield et al. 1979; Moser and Dutton 1988). The data presented in this article do, however, show that PF-QNM has the potential to investigate novel aspects of the formation, nature and dissociation of cyt c_2–RC-LH1-PufX interactions, on time-scales relevant to the in vivo processes in bacterial membranes.

In contrast, during our SMFS experiments the tip–sample contact time is in the range 2–4 ms and the repetition rate is 1 Hz. The former parameter is at least an order of magnitude larger that the half-life of the bound state, while the latter is two orders of magnitude lower than the turnover rate of the cyt c_2. In such circumstances, the molecules have time to unbind spontaneously prior to the application of an external force, thus not allowing measurements of either the actual binding probability, but instead providing an apparent value, which can differ substantially from the actual value. This is evident in our experimental results—a 66 % binding frequency was obtained from QNM data and 29 % (for single RC-LH1-PufX–cyt c_2 contacts) from SMFS data. It is worth noting that the 'binding efficiency' between the oxidised RC-His$_{12}$-LH1-PufX and the reduced cyt c_2-His$_6$ molecules when forming the electron transfer complex is limited both by the tethered nature of the molecules restricting their mobility and the possibility for spontaneous unbinding.

A single RC-LH1-PufX core complex can accept an electron from only one cyt c_2 at a time even if there are many reduced cytochromes on the AFM probe that can be brought into contact with the core complex. Also bringing the oxidised RC-LH1-PufX and the reduced cyt c_2 molecules together still does not guarantee the formation of an electron transfer complex mainly because of the restricted mobility and improper orientation (although the His-tag gives some control over the orientation still does not

guarantee perfect orientation of the docking sites) of the tethered molecules.

With these considerations in mind, we can be confident that the unbinding events recorded in the nano-mechanical adhesion images result from the unbinding interactions arising between single cyt c_2–RC-LH1-PufX pair, especially since the core complexes are widely spaced out on the sample surface. The situation changes with an increased density of core complexes on the sample surface, as in our SMFS experiments. In the force distribution histogram compiled from the SMFS data there is a double peak with a higher force value of 305 ± 25 pN which is approximately (within the error of the measurement) twice as high as the lower force of 164 ± 19 pN. This most probably indicates that this particular series of force–distance curves also recorded the interactions between pairs of core complexes interacting with pairs of cytochromes on the AFM probe. The difference in the unbinding force values obtained from PF-QNM measurements, $\sim$480 pN, and from SMFS measurements, $\sim$160 pN, for the single cyt c_2–RC-LH1-PufX electron transfer complex are unrelated to the low repetition rates for SMFS, but are a consequence of the vastly different loading rates, which are two orders of magnitude higher for the PF-QNM measurements.

Finally, it is worth noting that the mixed EG_3/Ni^{2+}-NTA SAMs we used on the gold substrates helped to minimise the non-specific interaction between the cyt c_2 molecules on the AFM probe and the sample surface as the majority of the gold sample surface is covered with adhesion-resistant PEG end-groups (Vanderah et al. 2004) and this is evident from the very low probability for non-specific interactions in our SMFS data (Fig. 5d).

Conclusion

This article presents a simple and reliable scanning probe methodology for quantifying the intermolecular forces between single molecules of a membrane protein and its extrinsic partner, in this case the cyt c_2–RC-LH1-PufX electron donor/acceptor pair. The thousands of force curves recorded using the PF-QNM method yield robust measurements of intermolecular forces. Furthermore, these and other such interactions can be used as the basis for nano-scale mapping of membrane proteins, overcoming the problem of identifying proteins in high-resolution AFM topography images.

References

Axelrod HL, Okamura MY (2005) The structure and function of the cytochrome c_2: reaction center electron transfer complex from *Rhodobacter sphaeroides*. Photosynth Res 85:101–114

Berquand A, Xia N, Castner DG, Clare BH, Abbott NL, Dupres V, Adriaensen Y, Dufrêne YF (2005) Antigen binding forces of single antilysozyme Fv fragments explored by atomic force microscopy. Langmuir 21:5517–5523

Bonanni B, Kamruzzahan ASM, Bizzarri AR, Rankl C, Gruber HJ, Hinterdorfer P, Cannistraro S (2005) Single molecule recognition between cytochrome C 551 and gold-immobilized azurin by force spectroscopy. Biophys J 89:2783–2791

Chen X-Y, Yurkov V, Paddock M, Okamura M, Beatty JT (1998) A *puhA* gene deletion and plasmid complementation system for site directed mutagenesis studies of the reaction center H protein of *Rhodobacter sphaeroides*. Photosyn Res 55:369–373

Chiu J, March PE, Lee R, Tillett D (2004) Site-directed, ligase-independent mutagenesis (SLIM): a single-tube methodology approaching 100% efficiency in 4 h. Nucl Acids Res 32:e174

Chtcheglova LA, Waschke J, Wildling L, Drenckhahn D, Hinterdorfer P (2007) Nano-scale dynamic recognition imaging on vascular endothelial cells. Biophys J 93:L11–L13

Comayras F, Jungas C, Lavergne J (2005) Functional consequences of the organization of the photosynthetic apparatus in *Rhodobacter sphaeroides*. I. Quinone domains and excitation transfer in chromatophores and reaction center antenna complexes. J Biol Chem 280:11203–11213

Conti M, Falini G, Samorì B (2000) How strong is the coordination bond between a histidine tag and Ni–nitrilotriacetate? An experiment of mechanochemistry on single molecules. Angew Chem Int Ed 39:215–218

Dupres V, Menozzi FD, Locht C, Clare BH, Abbott NL, Cuenot S, Bompard C, Raze D, Dufrêne YF (2005) Nanoscale mapping and functional analysis of individual adhesins on living bacteria. Nat Methods 2:515–520

Dutton PL, Prince RC (1978) In: Clayton RK, Sistrom WS (eds) The photosynthetic bacteria. Plenum Press, New York, pp 525–570

Ebner A, Kienberger F, Kada G, Stroh CM, Geretschläger M, Kamruzzahan ASM, Wildling L, Johnson WT, Ashcroft B, Nelson J, Lindsay SM, Gruber HJ, Hinterdorfer P (2005) Localization of single avidin–biotin interactions using simultaneous topography and molecular recognition imaging. Chem Phys Chem 6:897–900

Fotiadis D, Scheuring S, Engel A, Müller DJ (2002) Imaging and manipulation of biological structures with the AFM. Micron 33:385–397

Gerencsér L, Laczkó G, Maróti P (1999) Unbinding of oxidized cytochrome c from photosynthetic reaction center of *Rhodobacter sphaeroides* is the bottleneck of fast turnover. Biochemistry 38:16866–16875

Hinterdorfer P, Dufrêne YF (2006) Detection and localization of single molecular recognition events using atomic force microscopy. Nat Methods 3:347–355

Ludwig M, Dettmann W, Gaub HE (1997) AFM imaging contrast based on molecular recognition. Biophys J 72:445–448

Moser CC, Dutton PL (1988) Cytochrome c and c_2 binding dynamics and electron transfer with photosynthetic reaction center protein and other integral membrane redox proteins. Biochemistry 27:2450–2461

Müller DJ, Dufrêne YF (2008) Atomic force microscopy as a multifunctional molecular toolbox in nanobiotechnology. Nat Nanotechnol 3:261–269

Nevo R, Stroh C, Kienberger F, Kaftan D, Brumfeld V, Elbaum M, Reich Z, Hinterdorfer P (2003) A molecular switch between alternative conformational states in the complex of Ran and Importin β1. Nat Struct Biol 10:553–557

Overfield RE, Wraight CA, Devault D (1979) Microsecond photooxidation kinetics of cytochrome c_2 from *Rhodopseudomonas sphaeroides*: in vivo and solution studies. FEBS Lett 105:137–142

Paddock ML, Rongey SH, Abresch EC, Feher G, Okamura MY (1988) Reaction centers from three herbicide resistant mutants of *Rhodobacter sphaeroides* 2.4.1: sequence analysis and preliminary characterization. Photosynth Res 17:75–96

Patent US (2010)/0122385 A1, Method and apparatus of operating a scanning probe microscope

Pogorelov TV, Autenrieth F, Roberts E, Luthey-Schulten Z (2007) Cytochrome c_2 exit strategy: dissociation studies and evolutionary implications. J Phys Chem B 111:618–634

Scheuring S, Boudier T, Sturgis JN (2007) From high-resolution AFM topographs to atomic models of supramolecular assemblies. J Struct Biol 159:268–276

Schmidt JJ, Jiang X, Montemagno CD (2002) Force tolerances of hybrid nanodevices. Nano Lett 2:1229–1233

Simon R, Preifer U, Puhler A (1983) A broad host range mobilization system for in vivo genetic engineering: transposon mutagenesis in Gram negative bacteria. Nat Biotechnol 1:784–791

Sturgis JN, Tucker JD, Olsen JD, Hunter CN, Niederman RA (2009) Atomic force microscopy studies of native photosynthetic membranes. Biochemistry 48:3679–3698

Tehrani A, Prince RC, Beatty JT (2003) Effects of photosynthetic reaction center H protein domain mutations on photosynthetic properties and reaction center assembly in *Rhodobacter sphaeroides*. Biochemistry 42:8919–8928

Tetreault M, Rongey SH, Feher G, Okamura MY (2001) Interaction between cytochrome c_2 and the photosynthetic reaction center from *Rhodobacter Sphaeroides*: effects of charge-modifying mutations on binding and electron transfer. Biochemistry 40:8452–8462

Vanderah DJ, La H, Naff J, Silin V, Rubinson KA (2004) Control of protein adsorption: molecular level structural and spatial variables. J Am Chem Soc 126:13639–13641

Verbelen C, Gruber HJ, Dufrêne YF (2007) The NTA–His6 bond is strong enough for AFM single-molecular recognition studies. J Mol Recognit 20:490–494